J Biosci (2022)47:26
DOI: 10.1007/s12038-022-00261-y

Mean residence times of TF-TF and TF-miRNA toggle switches

KUHELI BISWAS[1]*, MOHIT KUMAR JOLLY[2] and ANANDAMOHAN GHOSH[1]

[1]*Indian Institute of Science Education and Research Kolkata, Mohanpur, Nadia 741 246, India*

[2]*Centre for BioSystems Science and Engineering, Indian Institute of Science, Bengaluru 560 012, India*

**Corresponding author (Email, kb15ip016@iiserkol.ac.in)*

MS received 4 October 2021; accepted 26 January 2022

Toggle switch networks are the simplest possible circuits with the ability of making a decision related to cell differentiation during embryonic development and disease progression. A common occurrence of toggle switch circuits is in the epithelial–mesenchymal transition (EMT) and its reverse, the mesenchymal–epithelial transition (MET), pathways which play key roles in phenotypic plasticity during cancer metastasis and therapy resistance. Recent studies have shown that the cells attaining one or more hybrid epithelial/mesenchymal (E/M) phenotypes during EMT/MET are more aggressive than those in either the epithelial or mesenchymal phenotype. In this work we studied the stability of each phenotype for different toggle switch circuits. We considered two-component toggle switch networks comprising either two mutually inhibiting transcription factors (TF-TF) or a TF-microRNA (TF-miR) chimera pair, and from Langevin dynamics, we determined the mean residence time (MRT) of cell phenotypes. MRT can be considered to be an indicator of stability in each cell phenotype and we showed that by replacing one of the TFs of the TF-TF toggle switch with miRNA generically stabilizes the hybrid phenotype. However, in the absence [presence] of a monostable hybrid state, the miRNA with faster [slower] degradation will make the hybrid state more probable. These results help to understand the implications of TF-TF and TF-miR circuits in the dynamics of cell fate decisions.

Keywords. Mean residence time; miRNA; stability of cell phenotype; stochastic modeling; toggle switch network

1. Introduction

Understanding cell fate decisions during embryonic development and tumorigenesis poses a major research challenge in modern developmental and cancer biology (Balázsi *et al.* 2011). The expression levels of various transcription factors (TFs) and microRNAs (miRNAs) that regulate cascades of regulatory networks change during cell fate determinations, generating genome-wide gene expression patterns corresponding to a particular cell lineage. The decision networks involved in cell fate determinations have a convoluted architecture depending on the biological context (Laslo *et al.* 2006; Kim *et al.* 2012). The core two-component circuits in many decision modules have the architecture of the classical TF-TF toggle switch, a regulatory motif in which the proteins of two genes act as mutually inhibiting TFs. Typically, one or both genes also act as self-activating TFs (directly or through other genes), thus forming a 'self-activating toggle switch' (SATS). Two well-studied examples are the PU1-GATA1 pair (Duff *et al.* 2012), which governs the differentiation of a common myeloid progenitor into two different hematopoietic lineages, and the CDX2-OCT3/4 pair (Niwa *et al.* 2005), which is associated with the differentiation of embryonic stem (ES) cells.

Besides the two-component TF-TF circuit, it has been well established that translational regulation by miRNA plays a crucial role during embryonic development and tumorigenesis (Esquela-Kerscher and Slack 2006; Ivey and Srivastava 2010; Jia *et al.* 2017) and many of the decision modules encompass miRNAs (Martinez and Walhout 2009). In particular,

This article is part of the Topical Collection: Emergent dynamics of biological networks.

Published online: 20 April 2022

Table 1. Parameter value of TF-miR chimera toggle switch, with and without the self-activating transcription factor (Lu *et al.* 2013)

Network	Production rates (molecules/minute)	Degradation rates (minute^{-1})	Hill threshold (molecules)
TF-miR chimera TS	$g_{\mu,0} = 0.6$ $g_{\mu,B} = 0.1$ $g_{\mu,I} = 5.4$ $g_m = 30$	$k_\mu = 0.01$ $k_m = 0.1$ $k_B = 0.2$	$\mu_0 = 100$ $B_0^\mu = 600$ $I_0 = 50$ $n_\mu = 6$ $n_I = 2$
TF-miR chimera TS with asymmetric SA	$g_{\mu,0} = 0.6$ $g_{\mu,B} = 0.1$ $g_{\mu,I} = 5.4$ $g_{m,0} = 6$ $g_{m,B} = 24$	$k_\mu = 0.01$ $k_m = 0.1$ $k_B = 0.2$	$\mu_0 = 100$ $B_0^\mu = 600$ $B_0^m = 200$ $I_0 = 50$ $n_\mu = 6$ $n_I = 2$

Table 2. Parameter values corresponding to miRNA-mediated translation and degradation of mRNA and miRNA (Lu *et al.* 2013)

Translation	minute^{-1}	mRNA degradation	minute^{-1}	miRNA degradation	minute^{-1}
l_0	1	$\gamma_{\mu 1}$	0.0002	γ_{m1}	0.005
l_1, l_2	0.5	$\gamma_{\mu 2}$	0.0002	γ_{m2}	0.005
$l_1 2$	0.05	$\gamma_{\mu 12}$	0.002	γ_{m12}	0.00

Table 3. Parameter value of TF-TF toggle switch, with and without the self-activating gene (Lu *et al.* 2013)

Network	Production rates (molecules/minute)	Degradation rates (minute^{-1})	Hill threshold (molecules)
TF-TF TS	$g_{A,0} = 10$ $g_{A,I} = 100$ $g_{A,B} = 2$ $g_{A,IB} = 10$	$k_A = 0.1$ $k_B = 0.1$	$A_0^B = 200$ $B_0^A = 200$ $I_0^A = 50$ $n_{A_B} = 4$ $n_{B_A} = 4$ $n_{I_A} = 2$
TF-TF TS with asymmetric SA	$g_{A,0} = 1$ $g_{A,I} = 50$ $g_{A,B} = 0.1$ $g_{A,IB} = 1$ $g_{B,0} = 3$ $g_{B,B} = 50$	$k_A = 0.1$ $k_B = 0.1$	$A_0^B = 100$ $B_0^A = 240$ $B_0^B = 80$ $I_0^A = 50$ $n_{A_B} = 1$ $n_{B_A} = 5$ $n_{B_B} = 4$ $n_{I_A} = 2$

'translation–transcription chimera' toggle switches comprising miRNA-TF pairs are found to play an important role in fate determination by cancer cells. For instance, the Lin28-let-7 pair forms such a switch that is associated with the regulation of self-renewal of cancer stem cells (Yang *et al.* 2010). The well-studied miR-200, miR-128-2, and miR-34 form chimera switches with SNAIL, ZEB1/2, and GATA3, TFs that regulate the epithelial–mesenchymal transition (EMT) (Bracken *et al.* 2008; Burk *et al.* 2008; Siemens *et al.* 2011; Yang *et al.* 2011; Qian *et al.* 2012) and the reverse transition, the mesenchymal–epithelial transition (MET). In the TF-miR chimera toggle switch network, it is often found that the gene

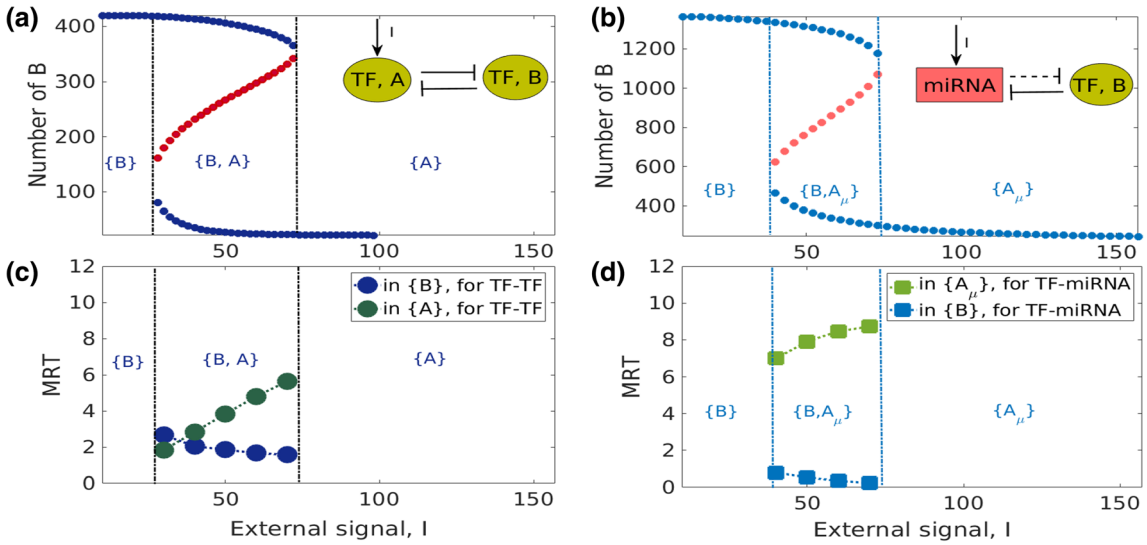

Figure 1. Bistable regime: Schematic representation and bifurcation diagram of (**a**) TF-TF and (**b**) TF-miRNA chimera toggle switch circuits in the presence of an external signal *I*. In the inset of (**a**) and (**b**), the solid green circle denotes the transcription factor, whereas the red square box denotes miRNA. The solid black bar and arrow, respectively, denote transcriptional inhibition and activation, whereas the dashed black bar denotes niRNA-mediated translational regulation. (**a** and **b**) Bifurcation diagram as a function of external signal *I*, where the red shaded circles denote unstable points and blue shaded circles correspond to the stable points. Variation of MRT with external signal *I* for (**c**) TF-TF and (**d**) TF-miRNA toggle switch networks.

acts as a self-activating TF, referred to as an 'asymmetric self-activating chimera toggle switch'. These simple TF-TF and TF-miR chimera toggle switch circuits with or without self-activation are embedded in more elaborate decision modules in the context of both ES cells and cancer cells (Chickarmane *et al.* 2006; Choi *et al.* 2011; Gregory *et al.* 2011; Polytarchou *et al.* 2012; Qian *et al.* 2012; Hill *et al.* 2013).

In this study, we considered the toggle switch networks and investigated the impact of miRNA stability on the stability of cell phenotypes by computing the mean residence time (MRT), the average time spent by the cells in a particular state. Thus, the phenotype with a larger MRT implies relatively higher stability in comparison with other co-existing phenotypes/states (Biswas *et al.* 2019; Subbalakshmi *et al.* 2020, 2021). The different phenotypic states of the system are: $\{B\}$ (high TF-B, low TF-A or low miRNA); $\{A\}$ or $\{A_\mu\}$ (low TF-B, high TF-A or high miRNA) labeled by the molecule present in abundance; and a hybrid state $\{P\}$ has intermediate numbers of TF-B and TF-A or miRNA molecules.

First, we started with a simpler bistable TF-TF toggle switch network and computed the stability of cell phenotypes $\{B\}$ and $\{A\}$. We then replaced one of those TFs with an miRNA and again computed the stability of cell phenotypes $\{B\}$ and $\{A_\mu\}$. For the TF-miR toggle switch, the MRT of phenotype $\{B\}$ $[\{A_\mu\}]$ is less [more] as compared with the TF-TF toggle switch, i.e., in the presence of miRNA, cells are less [more] prone to stay in the $\{B\}$ $[\{A_\mu\}]$ state.

Second, we compared the stability of cell phenotypes between the asymmetric self-activating TF-TF and TF-miR toggle switches, which can typically have three stable states: $\{B\}$, $\{A\}$ for TF-TF or $\{A_\mu\}$ for TF-miR, and $\{P\}$. In agreement with the previous result, even in the presence of self-activation, miRNA stabilizes the newly emerging hybrid phenotype $\{P\}$ state and we suspect that the stability of miRNA may be the reason behind the stability of the $\{P\}$ state as the degradation rate of miRNA is less than that of the TFs. To verify our idea we computed MRT for a wide range of miRNA degradation rates, which surprisingly indicated that the cells prefer to stay in the hybrid state if the miRNA is less stable. Stable miRNA will make the hybrid phenotype more probable only when a monostable hybrid phenotype appears in the system.

2. Materials and methods

2.1 *Mathematical modeling*

TF-TF chimera toggle switch: The deterministic rate equations for the TF-TF toggle switch network in the

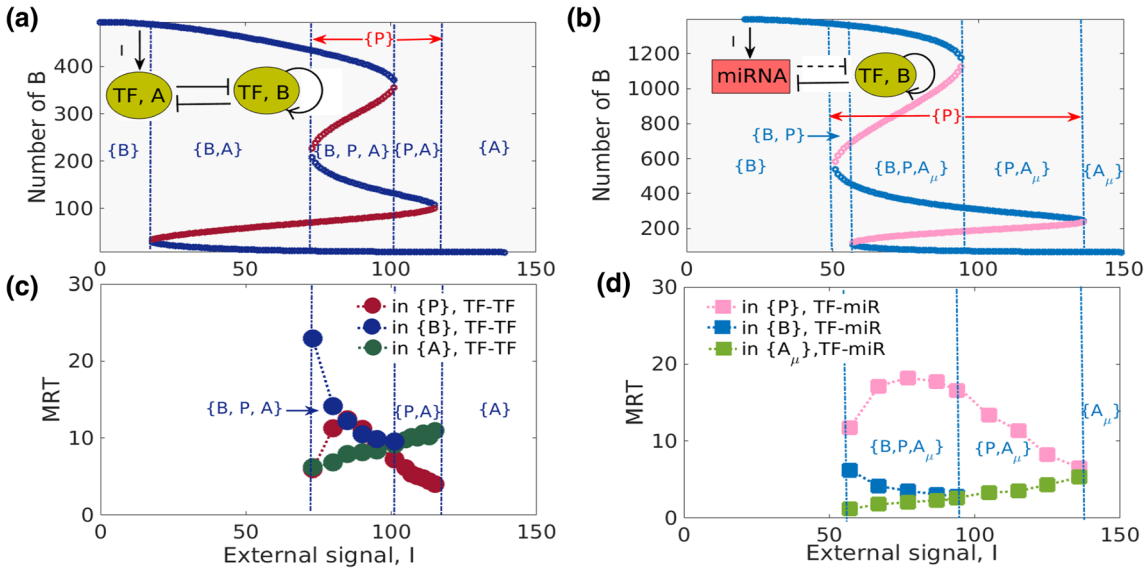

Figure 2. Tristable regime: Schematic representation and bifurcation diagram of (**a**) TF-TF and (**b**) TF-miRNA asymmetric self-activating chimera toggle switch circuits in the presence of an external signal I. In the inset of (**a**) and (**b**), the solid green circle denotes the transcription factor, whereas the red square box denotes miRNA. The solid black bar and arrow, respectively, denote transcriptional inhibition and activation, whereas the dashed black bar denotes niRNA-mediated translational regulation. (**a** and **b**) Bifurcation diagram as a function of external signal I, where the red shaded circles denote unstable points and blue shaded circles correspond to the stable points. Variation of MRT with external signal I for (**c**) TF-TF and (**d**) TF-miRNA asymmetric self-activating toggle switches.

presence of an external signal I (inset of figure 1a) are given as (Lu *et al.* 2013),

$$\begin{aligned}\dot{A} &= G_A(I,B) - k_A A,\\ \dot{B} &= g_{B0} + g_{BA}H^-(A) - k_B B,\end{aligned} \tag{1}$$

where the two TFs A and B have the degradation rates k_A and k_B, respectively. The general form of the effective production rate of the gene X that is regulated by the two TFs A and B in the case of two binding sites is given by

$$\begin{aligned}G_X(A,B) = (g_{X,0} - g_{X,A} - g_{X,B} + g_{X,AB})H^-(A)\\ H^-(B) + g_{X,AB}\\ + (g_{X,B} - g_{X,AB})H^-(A)\\ + (g_{X,A} - g_{X,AB})H^-(B),\end{aligned} \tag{2}$$

where the transcription rates for each promoter state are denoted by $g_{X,0}$, $g_{X,A}$, $g_{X,B}$, and $g_{X,AB}$. The illustration and description of the four states of the promoter are given by Lu *et al.* (2013). The general form for the inhibitory and excitatory one-TF Hill functions are

$$\begin{aligned}H^-(X) &= 1/[1 + (X/X_0)^{n_X}],\\ H^+(X) &= (X/X_0)^{n_X}/[1 + (X/X_0)^{n_X}] = 1 - H^-(X)\end{aligned} \tag{3}$$

TF-TF chimera toggle switch with asymmetric self activation: The deterministic rate equations for the asymmetric SATS network, involving two TFs A and B (inset of figure 2a) are given as (Lu *et al.* 2013)

$$\begin{aligned}\dot{A} &= G_A(I,B) - k_A A,\\ \dot{B} &= G_B(B,A) - k_B B\end{aligned} \tag{4}$$

TF-miR chimera toggle switch: The deterministic rate equations for the TF-miRNA toggle switch network, involving one TF and miRNA (inset of figure 1b) are given as (Lu *et al.* 2013)

$$\begin{aligned}\dot{\mu} &= G_\mu(I,B) - mY_\mu(\mu) - k_\mu \mu,\\ \dot{m} &= g_{m0} - mY_m(\mu) - k_m m,\\ \dot{B} &= mL(\mu) - k_B B,\end{aligned} \tag{5}$$

where I is the external signal acting on the miRNA μ, and k_μ, k_m, and k_B are the innate degradation rates of miRNA, mRNA, and protein of the gene B, respectively, and $G_\mu(I,B)$ is the effective production rate of the miRNA that is regulated by the TF B and external signal I. The expression for $G_\mu(I,B)$ is given by

$$\begin{aligned}G_\mu(I,B) = g_{\mu 0}H^-(I,B) + g_{\mu I}H^+(I,B)\\ + g_{\mu A}H^+(B,I),\end{aligned} \tag{6}$$

where the general form for the inhibitory and excitatory two-TF Hill functions is

$$\begin{aligned} H^-(I,B) &= 1/[1+(B/B_0)^{n_B}+(I/I_0)^{n_I}], \\ H^+(I,B) &= (I/I_0)^{n_I}/[1+(B/B_0)^{n_B}+(I/I_0)^{n_I}], \\ H^+(B,I) &= (B/B_0)^{n_B}/[1+(B/B_0)^{n_B}+(I/I_0)^{n_I}] \end{aligned} \tag{7}$$

In equation 5, g_{m0} is the transcription rate of mRNA, $mY_\mu(\mu)$ and $mY_m(\mu)$ are the miRNA-assisted degradation rates of the miRNA and mRNA, respectively, and $mL(\mu)$ is the miRNA-mediated translation of B given in Lu *et al.* (2013). From equation 5 we can see that miRNA inhibits TF-B in two ways: (i) by increasing the active degradation rate of mRNA, which is denoted by $Y_m(\mu)$, and (ii) by decreasing the translation rate of protein represented by $L(\mu)$. Hence, to incorporate these two mechanisms of inhibition of miRNA, the translation is modeled separately in the TF-miR toggle switch network. On the other hand, for the TF-TF toggle switch, the translation step is folded into an effective protein production rate (equation 4) because the two TFs inhibit each other only by repressing the translation step.

TF-miR chimera toggle switch with asymmetric self activation: The deterministic rate equations for the asymmetric SATS network, involving one TF B and miRNA μ (inset of figure 2b) are given as (Lu *et al.* 2013)

$$\begin{aligned} \dot{\mu} &= G_\mu(I,B) - mY_\mu(\mu) - k_\mu\mu, \\ \dot{m} &= g_{m,0} + g_{m,B}H^+(B) - mY_m(\mu) - k_m m, \\ \dot{B} &= mL(\mu) - k_B B \end{aligned} \tag{8}$$

where I is the external signal acting on the miRNA, k_μ, k_m, and k_B are the degradation rates of miRNA, mRNA, and the protein of the gene B, respectively, and $G_\mu(I,B)$ is the effective production rate of the miRNA μ that is regulated by two TFs B and I. The transcription rate of mRNA with B activation is $g_{m,0} + g_{m,B}H^+(B)$.

2.2 *Mean residence time analysis*

MRT was calculated as follows: we simulated the dynamical system in the presence of external noise which was assumed as Gaussian white noise and obtained the time evolution of the TF protein and miRNA using the Euler–Maruyama simulation (Kloeden and Platen 1992). The time evolution of molecules are, we assumed, in the following form:

$$\mathbf{x}(t+\Delta t) = \mathbf{x}(t) + F_1(\mathbf{x})\Delta t + \sqrt{2D\Delta t}\alpha_t$$

where α_t is a random number, chosen from the Gaussian distribution with mean 0 and variance 1. From the time evolution of the TF protein and miRNA, the dynamical states of the system are coarse-grained as an itinerary of basins visited. Then, MRT was calculated by multiplying the total number of successive states with Δt. The basin boundaries demarcate the different dynamical states of the system, namely, mesenchymal, epithelial, and hybrid E/M state. The typical basins of attraction for the tristable asymmetric TF-TF and TF-miRNA SATS are, respectively, given in the figures 13c and 14c. The numerical method involved the following steps (Biswas *et al.* 2019):

1. To calculate time evolution of TF and miRNA we used the Euler–Maruyama simulation of equation 5 with $\dot{m} = 0$ (as the degradation rate of mRNA is much faster as compared with that of the TF protein and miRNA, it will reach equilibrium faster). The time evolution of miRNA (x_1) and TF protein (x_2) assumes the forms

$$\begin{aligned} x_1(t+\Delta t) &= x_1(t) + F_1(x_1,x_2)\Delta t + \sqrt{2D\Delta t}\alpha_t, \\ x_2(t+\Delta t) &= x_2(t) + F_2(x_1,x_2)\Delta t + \sqrt{2D\Delta t}\beta_t \end{aligned} \tag{9}$$

α_t and β_t are random numbers chosen from a normal distribution with mean 0 and variance 1.
2. In the TF-miR plane the basin boundaries demarcate the different dynamical states of the system, namely, $\{B\}$, $\{A_\mu\}$, and $\{P\}$ states (figure 14c). From the time evolution of the TF protein and miRNA it is easy to coarse-grain the dynamical states of the system as an itinerary of basins visited. If we denote these three states by the symbols $\{B\}$, A_μ, and $\{P\}$, then the coarse-graining will yield a symbolic time series comprising a sequence of alphabets B, A_μ, and P.
3. Total number of successive Bs multiplied by Δt will give the residence time in $\{B\}$ state, and in the same way, number of successive Ps and A_μs multiplied by Δt will give residence time in $\{P\}$ and $\{A_\mu\}$ states, respectively. By taking the average of these residence times we can obtain the MRT for each phenotype.

3. Discussion

Toggle switch networks serve as core two-component circuits in many decision modules, especially related to cell differentiation during embryonic development and tumorigenesis. They are the simplest possible circuits with the ability to make a decision, either made of two TFs or a miRNA-TF pair. Previous bifurcation analyses of TF-TF and TF-miRNA toggle switches used a variety of deterministic equations and found several metastable states: $\{B\}$, $\{A\}$ for TF-TF/$\{A_\mu\}$ for TF-miR, and $\{P\}$ (hybrid) (Lu *et al.* 2013). This work considered the regulatory network of TF-TF and TF-miRNA toggle switches as a dynamical system and we quantified the stability properties of each metastable state. We compared the MRT of each stable state between the TF-TF and TF-miR toggle switch networks and by relating MRT with stability, we observed that miRNA stabilizes the hybrid phenotype of cells. Our analysis also showed that the miRNA degradation rate has a remarkable effect on the stability of hybrid phenotype: the unstable miRNA stabilizes the hybrid state of cells, and also the stable miRNA can also make the hybrid state more favorable only when the hybrid state exhibits monostability.

The TF-miR chimera toggle switch, with a self-activating gene, appears in the core EMT gene regulatory network, showing phenotypic plasticity during metastasis (Bracken *et al.* 2008; Yang *et al.* 2010; Nieto *et al.* 2016). During EMT, epithelial cells lose cell–cell adhesion and completely gain migratory traits, leading to a mesenchymal state, or with partial gain resulting in a hybrid E/M state. These hybrid E/M cells can be more metastatic than cells in epithelial or mesenchymal states (Pastushenko and Blanpain 2019; Jolly *et al.* 2018) and can exhibit collective cell migration as clusters of circulating tumor cells (CTCs) (Bocci *et al.* 2019; Campbell *et al.* 2019; Liao and Yang 2020), the major drivers of metastasis (Giuliano *et al.* 2018). Recent *in vitro*, *in vivo*, and *in silico* investigations have emphasized the existence and significance of hybrid E/M phenotype(s) in various cancer types (Jolly and Celià-Terrassa 2019). Interestingly, even a very small percentage of hybrid E/M cells (score $> 2\%$) was found to be sufficient to confer poor prognosis (Godin *et al.* 2020). Thus, identifying mechanisms that can maintain cells in a hybrid E/M phenotype is of crucial importance, and our MRT analysis shows that miRNA stabilizes the hybrid E/M state. miRNA not only stabilizes the hybrid E/M state but its degradation rate also has a distinct effect on the stability of the hybrid E/M phenotype. With the TF-miR toggle switch network with asymmetric self-activation, we showed that the stability of the hybrid E/M phenotype decreases with the degradation rate of miRNA only when the monostable hybrid E/M state exists, but in the absence of the monostable hybrid E/M state, the stability of the hybrid E/M state increases with the degradation rate of miRNA, and this is true for any multistable region.

4. Results

4.1 *miRNA stabilizes the hybrid phenotype*

Bistable TF-TF and TF-miR chimera toggle switch: To determine the role of miRNA on the stability of the hybrid phenotype, we first investigated the dynamics of the TF-TF toggle switch network and then replaced one TF by miRNA and performed the dynamical analysis of the TF-miR toggle switch network. The gene regulatory networks of TF-TF and TF-miR toggle switch networks are given in the inset of figure 1a and b. The interactions between two TFs and TF-miRNA are captured through a set of coupled ordinary differential equations (ODEs) given in the materials and methods section (2.1).

First, we examined the steady-state behavior for both TF-TF and TF-miR toggle switches in response to the external signal I, as given in figure 1a and b, which shows that both networks can have two stable states, (0,1) and (1,0), where state (0) corresponds to relatively low expression (low concentration) and state (1) corresponds to relatively high expression. For the TF-TF toggle switch, we denote the state (TF-A$\equiv$0, TF-B$\equiv$1) as phenotype $\{B\}$ and (TF-A$\equiv$1, TF-B$\equiv$0) as phenotype $\{A\}$. Similarly, for TF-miR, the (miRNA$\equiv$0, TF-B$\equiv$1) state is denoted as $\{B\}$ and (miRNA$\equiv$1, TF-B$\equiv$0) is represented as $\{A_\mu\}$ phenotype. Thus, we have labeled the phenotypic states after the molecule present in abundance in that state. Interestingly, the steady-state value of TF protein levels are higher in the TF-miR toggle switch network as compared with the TF-TF toggle switch. Next, we compared the bifurcation diagram of the TF-TF network (figure 1a) with that of the TF-miR network (figure 1b) to determine the changes in the system behavior conferred by miRNA. In the presence of miRNA, a higher value of I, i.e., a stronger external signal, is required for the cells to

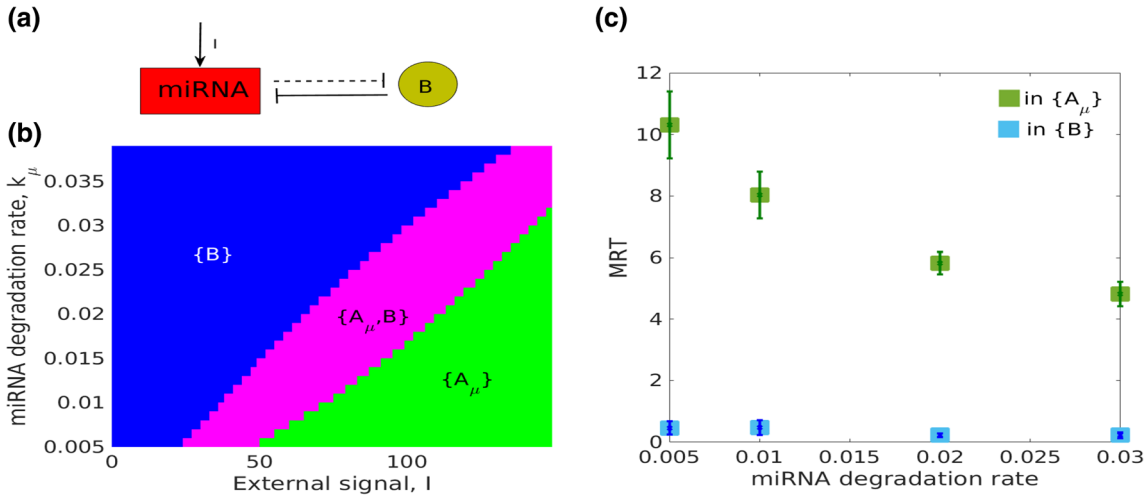

Figure 3. (**a**) Schematic representation of a TF-miRNA chimera toggle switch circuit in the presence of external signal, *I*. (**b**) Phase diagram of the TF-miRNA chimera toggle switch network when driven by an external signal *I* and miRNA degradation rate k_μ. The blue and green regions, respectively, denote monostable states $\{B\}$ and $\{A_\mu\}$, whereas the magenta region denotes the bistable state $\{A_\mu, B\}$. (**c**) Variation of MRT in $\{B\}$ (blue squares) and $\{A_\mu\}$ (green squares) phenotypes with miRNA degradation rate k_μ for the TF-miRNA chimera toggle switch network. The error bar denotes the variation of the MRT with the external signal *I*.

exit the $\{B\}$ phenotype, thus requiring a much stronger stimulus for the transformation from $\{B\}$ to $\{A_\mu\}$ phenotype.

Finally, to compare the stability of each cell phenotype between the TF-TF and TF-miR toggle switch networks, we carried out the MRT analysis with the external signal level *I* and have presented the results in figure 1c and d. Interestingly, for both of the TF-TF and TF-miRNA toggle switch networks, the $\{B\}$ state is less stable, and $\{A\}$ for TF-TF or $\{A_\mu\}$ for TF-miR are more stable if the external signal is stronger. Nevertheless, the stability of phenotype $\{B\}$ is less and $\{A_\mu\}$ is more for the TF-miR network than those of the TF-TF network. So, putting together these results, one may infer that the presence of miRNA makes the phenotype $\{B\}$ less favorable, and the cells need a stronger external signal to exit from the $\{B\}$ state and transfer into the $\{A\}$ (TF-TF)/$\{A_\mu\}$ (TF-miR) phenotype.

Tristable TF-TF and TF-miR chimera toggle switch with asymmetric self-activation: Further, we considered the TF-TF and TF-miR chimera toggle switch with asymmetric self-activation and compared the MRT of cell phenotypes between these toggle switch networks. The gene regulatory networks of the TF-TF and TF-miR toggle switch network with asymmetric self-activation are given in the inset of figure 2a and b. The interaction between two TFs and one TF and one miRNA was captured through a set of coupled ODEs, as described in the materials and methods section (2.1).

The steady-state behavior of the cells in figure 2a and b show that, in the presence of self-activation, for both the TF-TF and TF-miR toggle switches, a third new stable hybrid phenotype ($\{P\}$) emerges, which has an intermediate level of TF-B and TF-A (TF-TF)/miRNA (for TF-miR). Next, we compared the bifurcation diagram of the TF-TF network with that of the TF-miR network in the presence of asymmetric self-activation to determine the changes in the system behavior conferred by miRNA (figure 2a and b). In the presence of miRNA, the cell maintains a hybrid phenotype over a broader range of *I* levels (compare the range of *I* levels indicated by the red arrows in figure 2a and b), and a higher value of *I*, i.e., a stronger external signal, is required for the cells to exit the $\{B\}$ phenotype, thus requiring a much stronger stimulus to undergo a complete $\{B\}$ to $\{A_\mu\}$ transition (the same as the bistable toggle switch).

Finally, to analyze the stability of each cell phenotype we performed the MRT analysis for both of the TF-TF and TF-miR toggle switch networks in the presence of asymmetric self-activation and plotted the results in figure 2c and d. Similar to the bistable toggle switches, in this case also a stronger external signal *I* can make the phenotype $\{B\}$ less stable and phenotype $\{A\}$/$\{A_\mu\}$ more stable. But the stability of the hybrid

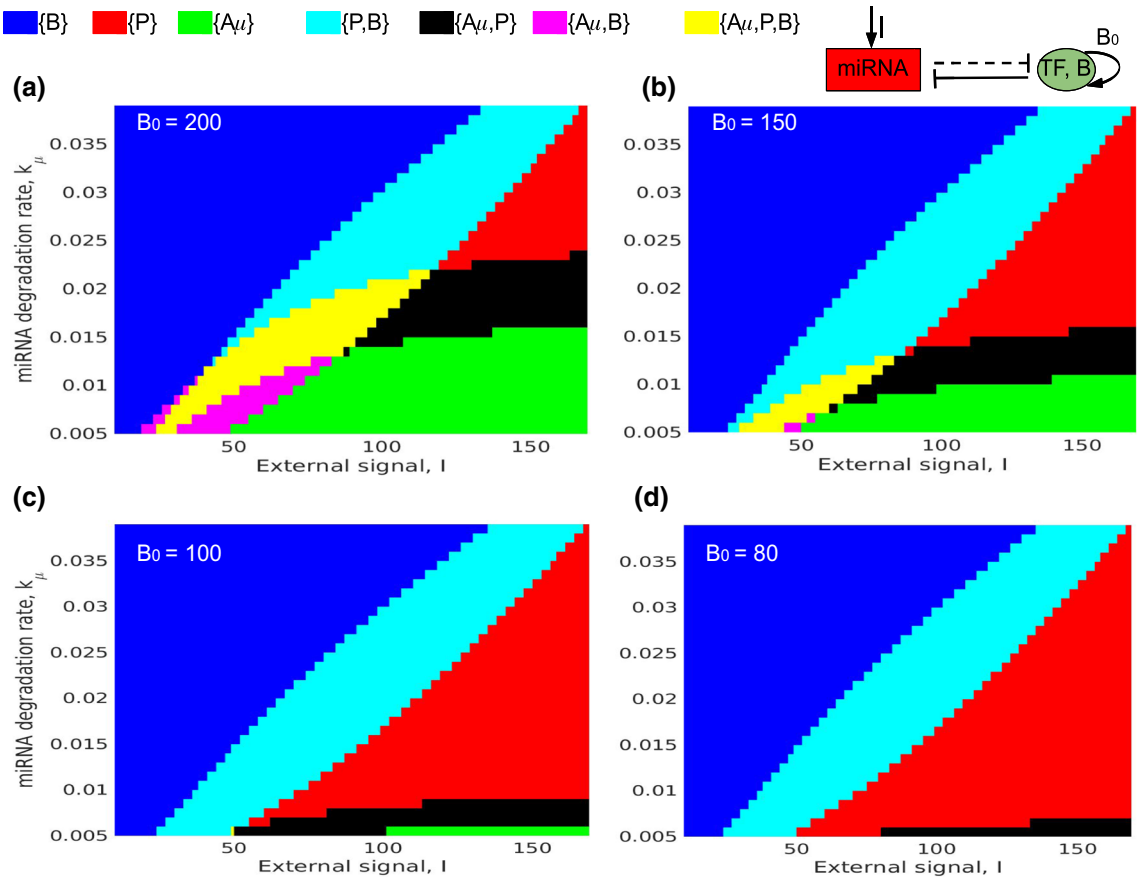

Figure 4. Phase diagram of the TF-miRNA asymmetric self-activating chimera toggle switch network when driven by an external signal I and miRNA degradation rate k_μ. The blue, green, and red regions, respectively, denote the monostable $\{B\}$, $\{E\}$, and hybrid $\{P\}$ states, whereas the yellow region denotes the tristable state $\{A_\mu, P, B\}$. For this circuit we get three types of bistable regions: (i)$\{A_\mu, B\}$, which is represented by the magenta region, (ii)$\{P, B\}$, represented by the cyan region, and (iii)$\{A_\mu, P\}$, represented by the black region. Here we have plotted the phase diagram for various strengths of the self-activating parameter B_0.

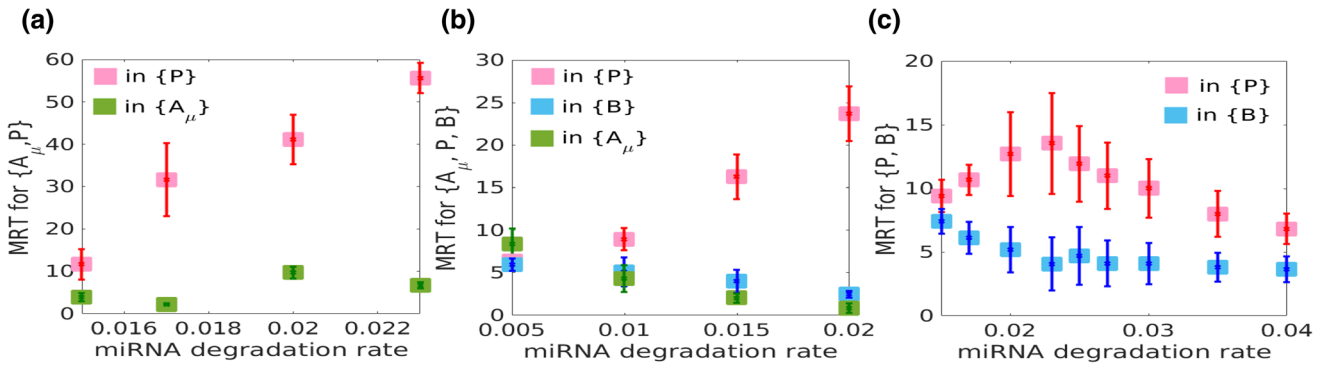

Figure 5. Variation of MRT with miRNA degradation rate k_μ in the (**a**) $\{A_\mu, P\}$, (**b**) $\{A_\mu, P, B\}$, and (**c**) $\{P, B\}$ multistable regions of the TF-miRNA asymmetric self-activating chimera toggle switch network with the strength of self-activating parameter $B_0 = 200$. The error bar denotes the variation of the MRT with the external signal I.

phenotype shows a non-monotonic behavior with the external signal I for both the TF-TF and TF-miR networks. Nevertheless, in the presence of self-activation, the MRT of the hybrid state is greater for the TF-miR network than that of the TF-TF network, which implies that the stability of the hybrid state can be increased if we replace one TF of the TF-TF toggle switch network with miRNA.

4.2 *TF-miR toggle switch: Stable miRNA increases the stability of* $\{A_\mu\}$ *state*

To understand the effect of miRNA stability on the stability of cell phenotype, we first investigated the effect of miRNA degradation rate on the steady state of TF-miRNA toggle switch network (figures 7 and 3b). The bifurcation plot shows that if we decrease the stability of miRNA, then a stronger external signal I is required to undergo a transition from $\{B\}$ to $\{A_\mu\}$ phenotypes. When the stability of miRNA is reduced, another key change is also noticed from figure 3b: the $\{B\}$ region expands while the $\{A_\mu\}$ region shrinks, but the spread of the bistable $\{A_\mu, B\}$ region between the monostable $\{B\}$ and $\{A_\mu\}$ states is almost uniform with the stability of miRNA. Put together, these results suggest that if the stability of miRNA is reduced (i.e., k_μ, the degradation rate of miRNA, is increased), the existence of a monostable $\{A_\mu\}$ is disfavoured, and a stronger external stimulus is required for complete $\{B\}$ to $\{A_\mu\}$ transition.

To observe the impact of miRNA degradation rate on the stability of cell phenotypes, we analyzed the MRT of each cell phenotype $\{B\}$ and $\{A_\mu\}$ within the $\{A_\mu, B\}$ bistable region. In figure 3c, we have plotted the variation of the MRT in the $\{B\}$ and $\{A_\mu\}$ states with the miRNA degradation rate k_μ, and it clearly shows that the MRT of $\{A_\mu\}$ decreases if we decrease the stability of miRNA. In this plot, the error bar denotes the variation of MRT with the external signal I. Put together, these observations from the phase plot and MRT plot suggest that if the stability of miRNA is reduced, the existence of a monostable $\{A_\mu\}$ phenotype is no more favorable and the stability of $\{A_\mu\}$ is also reduced, i.e., the probability of finding the cell in $\{A_\mu\}$ state is reduced.

4.3 *Asymmetric self-activating TF-miR toggle switch: Stable miRNA increases stability of hybrid phenotype only in the presence of monostable hybrid phenotype*

For further investigation of the effect of miRNA stability on the MRT of cell phenotypes, we considered the TF-miRNA chimera toggle switch network with asymmetric self-activation. First, we analyzed the effect of miRNA degradation rate on the steady-state of the TF-miRNA asymmetric self-activating chimera toggle switch network (figures 8 and 4a). From the bifurcation plot in figure 8, we can see that if we decrease the stability of miRNA, then a stronger external signal I is required to undergo a complete $\{B\}$ to $\{A_\mu\}$ transition, and after a certain degradation rate of miRNA, the $\{A_\mu\}$ state disappears. The phase plot in figure 4a also shows that if we reduce the stability of miRNA, then the $\{B\}$ region expands while the $\{A_\mu\}$ region shrinks, and after a certain value of miRNA degradation rate, the $\{A_\mu\}$ state completely disappears. Now, if we reduce the strength of the self-activation by reducing the parameter value B_0, then the self-activating chimera TF-miR toggle switch network (figure 2b) will converge into the TF-miR toggle switch network (figure 1b), which is also reflected in the plot of phase diagram (compare figures 4d and 3b). When the strength of the self-activation is reduced by keeping a fixed range of the external signal level and miRNA degradation rate, then one main change was noticed: the monostable $\{A_\mu\}$ state gradually disappears and a monostable hybrid state ($\{P\}$) appears even for a more stable miRNA (figure 4a–d). So, from the phase plots in figure 4, we can say that the existence of a monostable hybrid state is favorable if miRNA is less stable and the strength of the self-activating parameter is less.

The impact of miRNA durability on the stability of cell phenotypes was our main interest and for that we analyzed the MRT of each cell phenotype, $\{B\}$, $\{A_\mu\}$, and hybrid ($\{P\}$), with respect to the degradation rate of miRNA. From the plot of MRT in figure 5 we can say that for the $\{A_\mu, P\}$ and $\{A_\mu, P, B\}$ multi-stable region, MRT of the hybrid state increases if we decrease the stability of miRNA (figure 5a and b). But the scenario is completely different for the $\{P, B\}$ multi-stable region, where MRT of the hybrid state shows non-monotonic behavior with the stability of miRNA (figure 5c). The important features reflected in the MRT plot for $\{P, B\}$ region are: (i) The MRT in the hybrid state will increase within the range of miRNA degradation rate for which no monostable hybrid state exists (compare figures 4a and 5c) and (ii) the value of miRNA degradation rate from which MRT of the hybrid state starts to decrease is the same from where the monostable hybrid state emerges (compare figures 4a and 5c). Furthermore, we extended the MRT analysis of the hybrid phenotype by varying the strength of the self-activating parameter B_0 and have shown the results in the figure 6. From the plots in figure 6, we can say that even for various self-activating parameters, the results are generic, i.e., (i) for the $\{A_\mu, P\}$ and $\{A_\mu, P, B\}$ multi-stable region, the

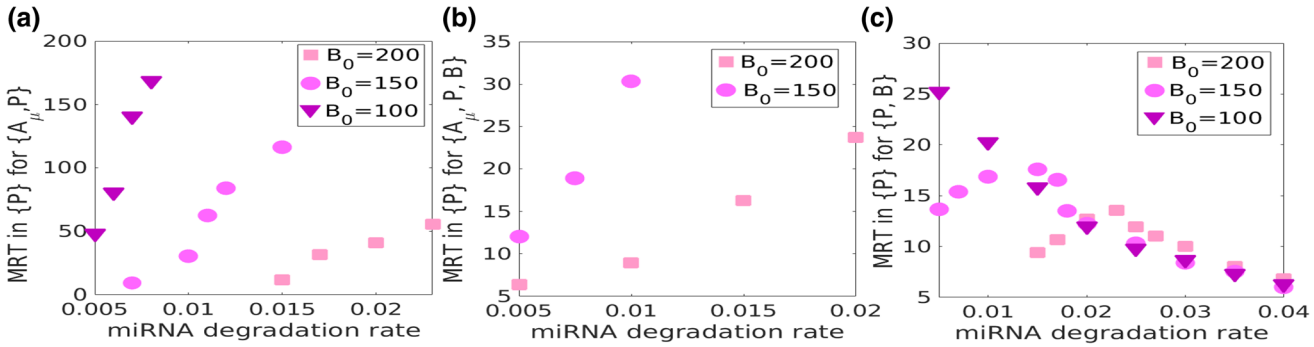

Figure 6. Variation of the MRT of the hybrid phenotype with miRNA degradation rate k_μ in the (**a**) $\{A_\mu, P\}$, (**b**) $\{A_\mu, P, B\}$, and (**c**) $\{P, B\}$ multi-stable regions of the TF-miRNA asymmetric self-activating chimera toggle switch network. Here we have plotted the MRT of the hybrid phenotype for various strengths of the self-activating parameter B_0.

stability of the hybrid state will increase if miRNA is less stable (figure 6a and b), and (ii) for the $\{P, B\}$ multi-stable region, the MRT of the hybrid state initially increases and then starts to decrease with miRNA degradation rate from the point where the monostable hybrid phenotype emerges.

From the TF-miR toggle switch networks with asymmetric self-activation, we can generally say that the stability of the hybrid phenotype will decrease with the degradation rate of miRNA only when a monostable hybrid state exists, but in the absence of a monostable hybrid state, the stability of the hybrid will increase with the degradation rate of miRNA, and this is true for any multi-stable region.

Acknowledgements

AMG would like to thank SERB, India, for the MATRICS grant MTR/2019/000232.

Appendix A: Bifurcation plot of TF-miR chimera toggle switch without and with asymmetric self-activation

In this section we provide the bifurcation diagrams of TF-miR chimera toggle switch networks with respect to external signal I for various degradation rates of miRNA (see figures 7–11).

Appendix B: Tristable TF-TF asymmetric SATS: Basin of attraction, bifurcation, and nullcline

Here, we have plotted the nullcline (figure 12a) and bifurcation diagrams (figure 12b and c) for the TF-TF asymmetric SATS network. We have also shown the dynamics of protein number of genes B and A in the presence of Gaussian white noise in figure 13a and b, respectively. In figure 13c we have plotted the basin of attraction which denotes each stable phenotype with

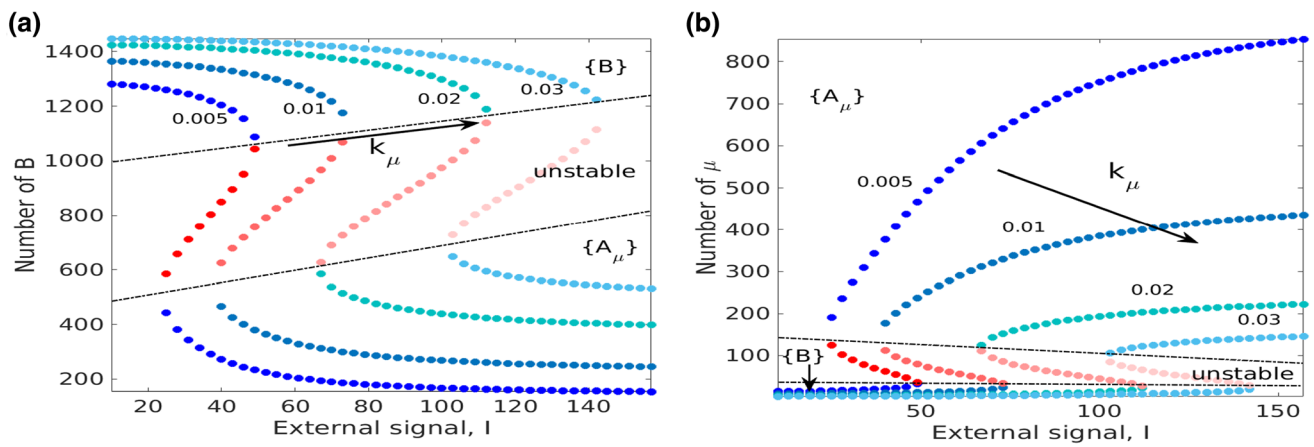

Figure 7. Bifurcation diagram as a function of input signal I for the simple TF-miRNA chimera toggle switch driven by an external signal I for various degradation rates of miRNA k_μ. The red shaded circles correspond to the unstable points and the blue shaded circles correspond to the stable point.

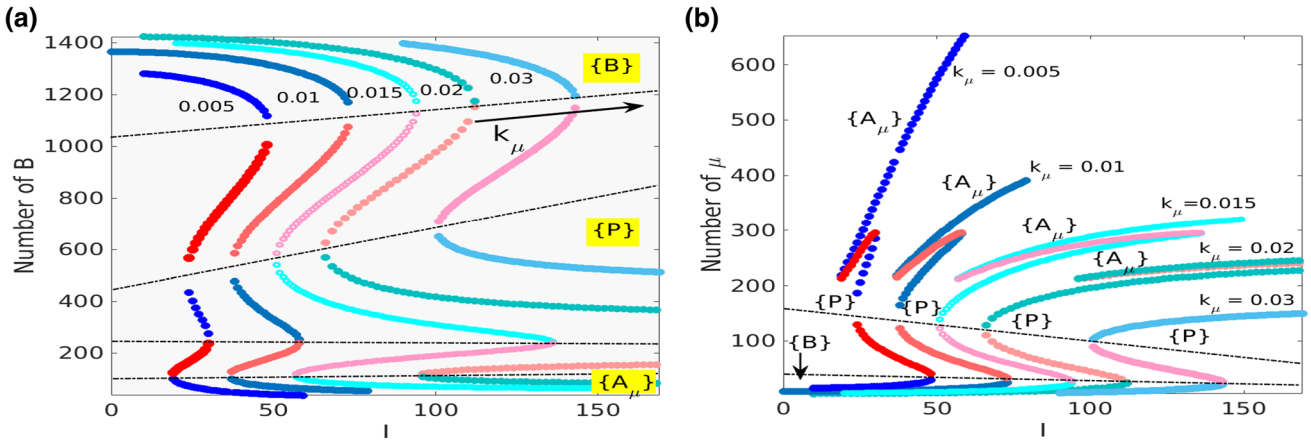

Figure 8. Bifurcation diagram as function of input signal I for the asymmetric self-activating TF-miRNA chimera toggle switch driven by an external signal I for various degradation rates of miRNA k_μ (corresponding to figure 4a). The red shaded circles correspond to the unstable points and the blue shaded circles correspond to the stable point.

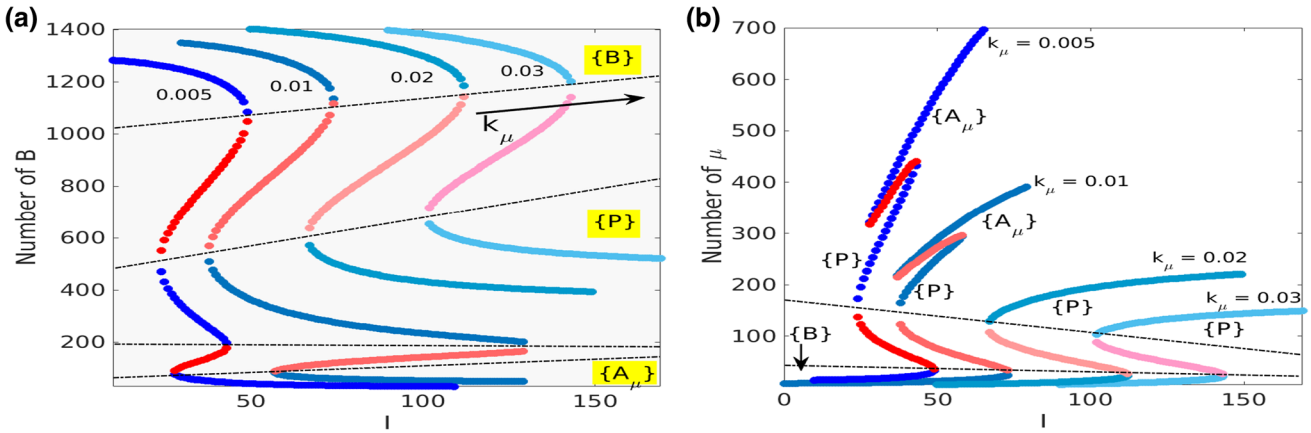

Figure 9. Bifurcation diagram as function of input signal I for $B_0 = 150$ (corresponding to figure 4b).

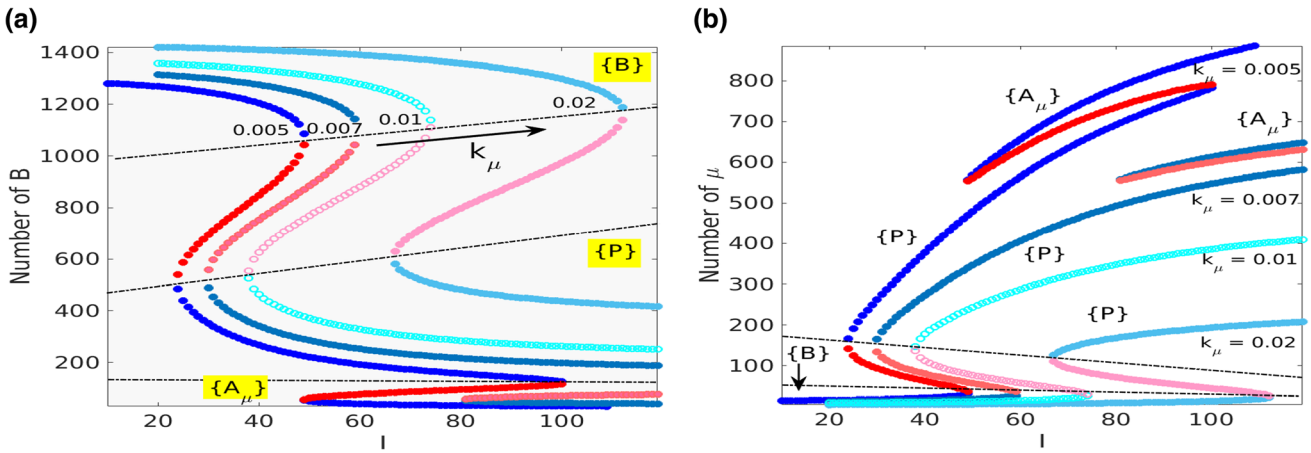

Figure 10. Bifurcation diagram as function of input signal I for $B_0 = 100$ (corresponding to figure 4c).

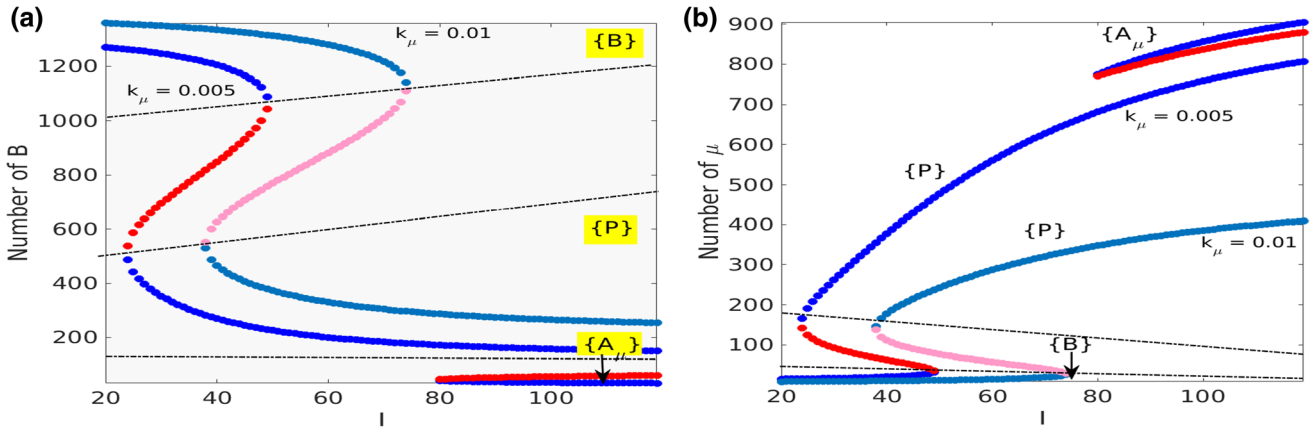

Figure 11. Bifurcation diagram as function of input signal I for $B_0 = 80$ (corresponding to figure 4d).

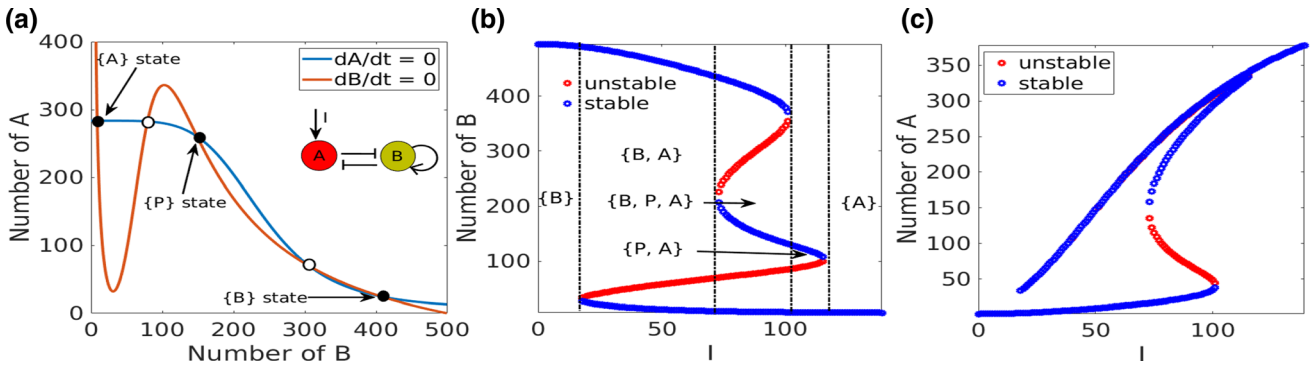

Figure 12. (**a**) Nullcline plots for the TF-TF asymmetric self-activating toggle switch for $I = 90$ molecules. The solid black [white] circles denote the stable [saddle] points. Bifurcation diagram of the level of (**b**) B and (**c**) A with respect to the external signal I.

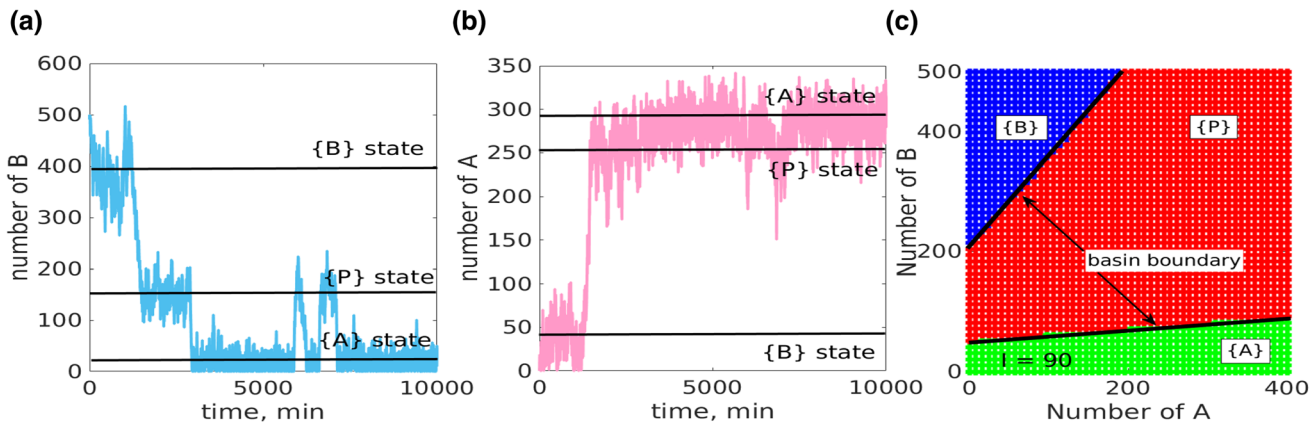

Figure 13. Stochastic time series of (**a**) TF-B and (**b**) TF-A for the TF-TF asymmetric SATS network showing switching between $\{A\}$, $\{B\}$, and $\{P\}$ states at $I = 90$ molecules. The solid black straight lines indicate the average values of A and B proteins for a given state and external signal strength $I = 90$ molecules. (**c**) Plot for the basin of attraction with basin boundaries for the TF-TF asymmetric SATS network with $I = 90$ molecules. Here, the blue, red, and green regions correspond to the $\{B\}$, hybrid, and $\{A\}$ states, respectively.

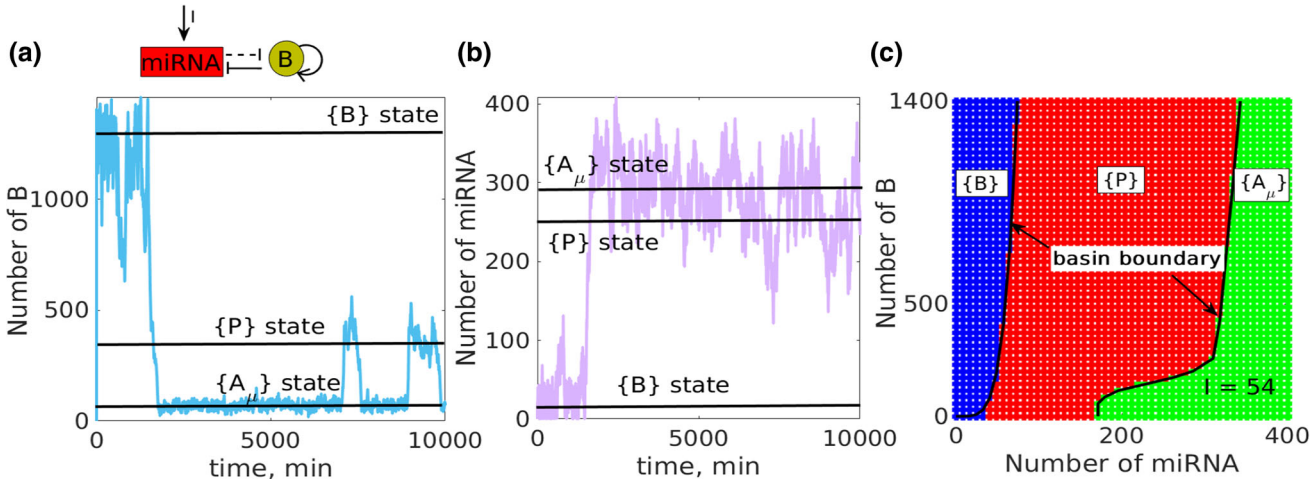

Figure 14. Stochastic time series of (**a**) TF-B and (**b**) miRNA for the TF-miRNA asymmetric SATS network showing switching between $\{A_\mu\}$, $\{B\}$ and $\{P\}$ states at $I = 54$ molecules. The solid black straight lines indicate the average values of B protein and miRNA for a given state and external signal strength $I = 54$ molecules. (**c**) Plot for the basin of attraction with basin boundaries for the TF-miRNA asymmetric SATS network with $I = 54$ molecules. Here, the blue, red, and green regions correspond to $\{B\}$, hybrid, and $\{A_\mu\}$ states, respectively.

basin boundaries (black lines). For the TF-TF asymmetric SATS we get three stable phenotypes: $\{B\}$ (gene A has low expression and gene B is highly expressed), $\{A\}$ (gene B has low expression and gene A is highly expressed), and $\{P\}$ (both genes A and B have intermediate levels of expression).

Appendix C: Tristable TF-miRNA asymmetric SATS: Basin of attraction

Here, we have plotted the basis of attraction (figure 14c) and stochastic dynamics of miRNA (figure 14b) and proteins (figure 14a) of gene B for the TF-miRNA asymmetric SATS network. In figure 14c we have plotted the basin of attraction which denotes each stable phenotype of cells along with the basin boundaries (black curves). For the TF-miR asymmetric SATS we get three stable phenotypes: $\{B\}$ (miRNA has low expression and gene B is highly expressed), $\{A_\mu\}$ (gene B has low expression and miRNA is highly expressed), and $\{P\}$ (both miRNA and gene B have intermediate levels of expression).

References

Balázsi G, van Oudenaarden A and Collins JJ 2011 Cellular decision making and biological noise: from microbes to mammals. *Cell* **144** 910–925

Biswas K, Jolly MK and Ghosh A 2019 Stability and mean residence times for hybrid epithelial/mesenchymal phenotype. *Phys. Biol.* **16** 025003

Bocci F, Jolly MK and Onuchic JN 2019 A biophysical model uncovers the size distribution of migrating cell clusters across cancer types. *Cancer Res.* **79** 5527–5535

Bracken CP, Gregory PA, Kolesnikoff N, *et al.* 2008 A double-negative feedback loop between ZEB1-SIP1 and the microRNA-200 family regulates epithelial-mesenchymal transition. *Cancer Res.* **68** 7846–7854

Burk U, Schubert J, Wellner U, *et al.* 2008 A reciprocal repression between ZEB1 and members of the miR-200 family promotes EMT and invasion in cancer cells. *EMBO Rep.* **9** 582–589

Campbell K, Rossi F, Adams J, *et al.* 2019 Collective cell migration and metastases induced by an epithelial-to-mesenchymal transition in *Drosophila* intestinal tumors. *Nat. Commun.* **10** 2311

Chickarmane V, Troein C, Nuber UA, Sauro HM and Peterson C 2006 Transcriptional dynamics of the embryonic stem cell switch. *PLoS Comput. Biol.* **2** e123

Choi YJ, Lin C-P, Ho JJ, *et al.* 2011 miR-34 miRNAs provide a barrier for somatic cell reprogramming. *Nat. Cell Biol.* **13** 1353–1360

Duff C, Smith-Miles K, Lopes L and Tian T 2012 Mathematical modelling of stem cell differentiation: the pu.1–gata-1 interaction. *J. Math. Biol.* **64** 449–468

Esquela-Kerscher A and Slack FJ 2006 Oncomirs–microRNAs with a role in cancer. *Nat. Rev. Cancer* **6** 259–269

Giuliano M, Shaikh A, Lo HC, *et al.* 2018 Perspective on circulating tumor cell clusters: why it takes a village to metastasize. *Cancer Res.* **78** 845–852

Godin L, Balsat C, Van Eycke Y-R, *et al*. 2020 A novel approach for quantifying cancer cells showing hybrid epithelial/mesenchymal states in large series of tissue samples: towards a new prognostic marker. *Cancers* **12** 906

Gregory PA, Bracken CP, Smith E, *et al*. 2011 An autocrine TGF-β/ZEB/miR-200 signaling network regulates establishment and maintenance of epithelial-mesenchymal transition. *Mol. Biol. Cell* **22** 1686–1698

Hill L, Browne G and Tulchinsky E 2013 ZEB/miR-200 feedback loop: at the crossroads of signal transduction in cancer. *Int. J. Cancer* **132** 745–754

Ivey KN and Srivastava D 2010 MicroRNAs as regulators of differentiation and cell fate decisions. *Cell Stem Cell* **7** 36–41

Jia D, Jolly MK, Harrison W, *et al*. 2017 Operating principles of tristable circuits regulating cellular differentiation. *Phys. Biol.* **14** 035007

Jolly MK and Celià-Terrassa T 2019 Dynamics of phenotypic heterogeneity associated with EMT and stemness during cancer progression. *J. Clin. Med.* **8** 1542

Jolly MK, Mani SA and Levine H 2018 Hybrid epithelial/mesenchymal phenotype (s): The 'fittest'for metastasis? *Biochim. Biophys. Acta Rev. Cancer* **1870** 151–157

Kim M-S, Kim J-R, Kim D, Lander AD and Cho K-H 2012 Spatiotemporal network motif reveals the biological traits of developmental gene regulatory networks in *Drosophila melanogaster*. *BMC Syst. Biol.* **6** 1–10

Kloeden PE and Platen E 1992 Higher-order implicit strong numerical schemes for stochastic differential equations. *J. Stat. Phys.* **66** 283–314

Laslo P, Spooner CJ, Warmflash A, *et al*. 2006 Multilineage transcriptional priming and determination of alternate hematopoietic cell fates. *Cell* **126** 755–766

Liao T-T and Yang M-H 2020 Hybrid epithelial/mesenchymal state in cancer metastasis: clinical significance and regulatory mechanisms. *Cells* **9** 623

Lu M, Jolly MK, Gomoto R, *et al*. 2013 Tristability in cancer-associated microRNA-TF chimera toggle switch. *J. Phys. Chem. B* **117** 13164–13174

Martinez NJ and Walhout AJ 2009 The interplay between transcription factors and microRNAs in genome-scale regulatory networks. *Bioessays* **31** 435–445

Nieto MA, Huang R Y-J, Jackson RA and Thiery JP 2016 EMT: 2016. *Cell* **166** 21–45

Niwa H, Toyooka Y, Shimosato D, *et al*. 2005 Interaction between Oct3/4 and Cdx2 determines trophectoderm differentiation. *Cell* **123** 917–929

Pastushenko I and Blanpain C 2019 EMT transition states during tumor progression and metastasis. *Trends Cell Biol.* **29** 212–226

Polytarchou C, Iliopoulos D and Struhl K 2012 An integrated transcriptional regulatory circuit that reinforces the breast cancer stem cell state. *Proc. Natl. Acad. Sci. USA* **109** 14470–14475

Qian P, Banerjee A, Wu Z-S, *et al*. 2012 Loss of SNAIL regulated miR-128-2 on chromosome 3p22. 3 targets multiple stem cell factors to promote transformation of mammary epithelial cells. *Cancer Res.* **72** 6036–6050

Siemens H, Jackstadt R, Hünten S, *et al*. 2011 miR-34 and SNAIL form a double-negative feedback loop to regulate epithelial-mesenchymal transitions. *Cell Cycle* **10** 4256–4271

Subbalakshmi AR, Kundnani D, Biswas K, *et al*. 2020 NFATc acts as a non-canonical phenotypic stability factor for a hybrid epithelial/mesenchymal phenotype. *Front. Oncol.* **10** 1794

Subbalakshmi AR, Sahoo S, Biswas K and Jolly MK 2021 A computational systems biology approach identifies SLUG as a mediator of partial epithelial-mesenchymal transition (EMT). *Cells Tissues Organs* **10** 1–14

Yang X, Lin X, Zhong X, *et al*. 2010 Double-negative feedback loop between reprogramming factor LIN28 and microRNA let-7 regulates aldehyde dehydrogenase 1–positive cancer stem cells. *Cancer Res.* **70** 9463–9472

Yang Y, Ahn Y-H, Gibbons DL, *et al.* 2011 The Notch ligand Jagged2 promotes lung adenocarcinoma metastasis through a miR-200–dependent pathway in mice. *J. Clin. Investig.* **121** 1373–1385

Corresponding editor: Susmita Roy